Ground-state shape phase transitions in nuclei: Thermodynamic analogy and finite-*N* effects

Pavel Cejnar,[1,2,*] Stefan Heinze,[2,†] and Jan Jolie[2,‡]
[1]*Institute of Particle and Nuclear Physics, Charles University, V Holešovičkách 2, 180 00 Prague, Czech Republic*
[2]*Institute for Nuclear Physics, University of Cologne, Zülpicherstr. 77, 50937 Cologne, Germany*
(Received 7 February 2003; published 23 September 2003)

We study quantum phase transitions between spherical, prolate, and oblate nuclear ground-state shapes using the interacting sd-boson model (sd-IBM) and demonstrate the analogy between the IBM results (also results of any axially symmetric quadrupole collective model) and predictions of the Landau theory of phase transitions in classical thermodynamics. A detailed comparison of the two frameworks is performed exploiting the concept of ''specific heat,'' introduced in four alternative ways in the quantum case. All these definitions (two of them based on spectroscopic features of the ground state, the others on a randomized version of the model) lead to similar peaked forms of the ''specific heat'' at the point of the quantum phase transition. We analyze the effect of an increasing boson number on these curves and observe convergence to the singular phase-transitional behavior in the classical limit. Other observable signatures of the IBM structural phase transitions are also discussed with the aim to facilitate the location of a particular nucleus in the parameter space (extended Casten triangle) near the transitions.

DOI: 10.1103/PhysRevC.68.034326 PACS number(s): 21.60.Fw, 21.10.Re, 05.70.Fh

I. INTRODUCTION

Phase transitions are a strongly discussed subject not only for traditional systems of condensed-matter physics, such as ferromagnetic and ferroelectric materials, solid and liquid crystals, or superfluid and superconducting media [1,2]. In nuclear physics, as well, phase transitions have attracted growing attention of both theorists and experimentalists for already several decades.

The most prominent—although not yet experimentally verified—phase transition in this field is the one from hadronic nuclear matter to the quark-gluon plasma [3]. At much lower, but still high enough energies, nuclear temperatures of about a few units of MeV, a phase transition similar to that between liquid and gas has been observed in the multifragmentation of nuclei in heavy-ion collisions [4]. In only a slightly lower temperature domain, variations of the form of giant dipole resonances observed in γ-ray spectra from hot rotating nuclei [5] indicate changes of the nuclear geometric shapes [6]. These observations seem to be in agreement with microscopic calculations of quadrupole shapes of nuclei [7], analyzed in the framework of Landau theory of phase transitions. By further descending to temperatures less than 1 MeV, another type of phase-transitional behavior is expected in nuclei, namely, the pairing transition between superconducting and normal phases [8].

The idea of phase transitions is so appealing that it is often imported from its homeland, classical thermodynamics, to other fields of physics. It was in this spirit when Thouless [9] used this term (still in quotation marks) to describe the situation, in which the ground-state wave function suddenly changes from one configuration to another under varying interaction constants in a quantum Hamiltonian. This situation is often referred to as quantum or structural phase transition [2]. One typically deals with a parameter-dependent quantum Hamiltonian

$$H(\lambda)=H_0+\lambda V\equiv(1-\lambda)H(0)+\lambda H(1) \tag{1}$$

with $\lambda\in[0,1]$ (any scaling coefficient can be absorbed in V), where the limits $H(0)$ and $H(1)$ represent two incompatible modes of motion, $[H(0),H(1)]\neq 0$. As documented by numerous examples [10–22], transitions between the limiting dynamical modes may have a crossover character, when the ground-state configuration (and in a limited extent also the structure of other states) flips suddenly from one form to another at a certain ''critical point'' $\lambda=\lambda_c$.

Note that the linearity of the dependence in Eq. (1) is not really essential for the phase-transitional behavior, although it considerably simplifies some important aspects of the analysis (as we will see below). We can, therefore, generalize Eq. (1) to nonlinear cases, when the Hamiltonian $H(\vec{\lambda})$ depends on a set of external parameters, $\vec{\lambda}=(\lambda_1,\lambda_2,\ldots,\lambda_f)$, in a general way, restricted just by the incompatibility condition

$$[H(\vec{\lambda}),H(\vec{\lambda}')]\neq 0 \quad \text{for } \vec{\lambda}\neq\vec{\lambda}'. \tag{2}$$

If $\vec{\lambda}$ varies along a continuous curve $\vec{\lambda}=\vec{\lambda}(t)$ in the parameter space, $t\in[0,1]$, the ground state can change abruptly at some $t=t_c$, in an apparent analogy with the linear case discussed above.

Since thermodynamic phase transitions can be both quantum and classical, we prefer using the name ''structural phase transition'' for the above-described situation (see, e.g., Ref. [13]). If the structure of only the ground state is looked for, these transitions correspond to the temperature $T=0$. Whereas thermodynamic quantum phase transitions (with T as a control parameter) concern only spectra of the systems subject to change (all observables being inherently contained in partition functions), the structural phase transitions are

*Electronic address: pavel.cejnar@mff.cuni.cz
†Electronic address: heinze@ikp.uni-koeln.de
‡Electronic address: jolie@ikp.uni-koeln.de

related to the form of energy eigenfunctions, i.e., to the very heart of quantum dynamics. In this sense they are indeed fundamentally different from thermodynamic phase transitions. By studying structural transitions in various toy and realistic systems [2,9–22], much insight has been gained during the past two decades concerning the essential features of quantum Hamiltonians that drive the systems to exhibit crossover behaviors.

In nuclear physics, the structural phase transition appears most commonly in two incarnations: the first concerns the superfluid (paired) and normal modes of motion in the nucleus [13,14,12,19], the second its various geometric forms [9–14,20,21,23–35]. In contrast to the previously discussed transitions between these phases in hot rotating nuclei, the present changes are induced by variations of the nuclear many-body Hamiltonian when going from one nucleus to another. In this paper, we will only be dealing with the ground-state shape phase transitions, our attention being mostly focused on properties of the interacting boson model (IBM) [36].

The plan of the paper is as follows: In Sec. II we review phase-transitional aspects of the quadrupole geometric model, interacting sd-boson model, and semimicroscopic Ginocchio and fermion dynamical-symmetry models. We believe that this part will illuminate important recent achievements and clarify some frequently asked questions in this field. In Sec. III, various spectroscopic signatures of transitions between spherical and deformed, and between prolate and oblate shapes are studied within the IBM. In particular, we compare the behavior of the ground-state energy and wave-function entropy, exploiting an analogy with classical thermodynamics via the concept of ''specific heat.'' In Sec. IV, we further extend this analogy by studying *thermal* properties of the IBM with control parameters subject to a small-amplitude random noise. The ''specific heat,'' which naturally appears in this stochastic version of the model, turns out to be closely related to that from Sec. III. All these approaches sum up in a picture that exhibits apparent analogies between structural phase transitions in the quantum bosonic system represented by the IBM and standard phase transitions in classical thermodynamics. We assume that these analogies can be further studied also in other systems with quantum phase transitions.

II. NUCLEAR SHAPE TRANSITIONS: AN OVERVIEW

A. Geometric model

A natural habitat for the description of nuclear shapes is the geometric model [37,38]. The geometric Hamiltonian must be a scalar and thus depends only on rotational invariants constructed from tensorial shape coordinates $\alpha^{(K)}$ and associated moments $\pi^{(K)}$. Usually, only the quadrupole deformations are taken into account, $K=2$, and the Hamiltonian is expanded such that it contains only few lowest-order invariants summed up with certain weight coefficients. As the potential energy does not depend on the orientation of the deformed shape in the laboratory system, it contains, in the quadrupole case, only the Hill-Wheeler intrinsic variables β and γ. With the above restrictions it reads as

$$V(\beta,\gamma)=A\beta^2+B\beta^3\cos 3\gamma+C\beta^4+\cdots \tag{3}$$

(where $A, B, C, \ldots$ are constants). Remind that β and γ are polar coordinates of the $\alpha_0^{(2)}$ and $\sqrt{2}\alpha_{\pm 2}^{(2)}$ components of diagonalized tensor of quadrupole variables. To allow for negative values of β (which will turn important below) we adopt here the convention with $\beta\in(-\infty,+\infty)$ and $\gamma\in[0,\pi)$.

The classical equilibrium configuration is given by the position $(\beta,\gamma)=(\beta_0,\gamma_0)$ of the global minimum of potential energy (3). The analysis becomes particularly simple if the higher-order terms can be truncated: In this case, C must be positive to ensure physical asymptotics of the potential. As the γ dependence in the truncated Eq. (3) allows only for $\gamma_0=0$ or $\pi/3$, where the latter case can be equivalently expressed by the substitutions $\gamma_0\mapsto 0$ and $\beta_0\mapsto-\beta_0$, we set $\gamma_0=0$ [34]. We therefore identify three types of equilibrium shapes: (i) spherical for $\beta_0=0$, (ii) prolate axisymmetric for $\beta_0>0$, and (iii) oblate axisymmetric for $\beta_0<0$. These apply for (i) $A>A_c$, (ii) $A<A_c$, $B<0$, and (iii) $A<A_c$, $B>0$, where the ''critical'' value of A is

$$A_c=\frac{B^2}{4C}. \tag{4}$$

If approaching A_c from below, the ''spherical minimum'' $\beta_0=0$ appears as a local minimum already for $A=0\equiv A_0\leqslant A_c$, but only at $A=A_c$ it becomes degenerated with the ''deformed minimum'' $\beta_0\neq 0$ and takes over the role of the global minimum. On the other hand, if approaching A_c from above, a deformed local minimum first appears for $A=9B^2/(32C)\equiv A_1\geqslant A_c$. The range $A\in[A_0,A_1]$ thus corresponds to a form of the potential with two minima, the deformed minimum being lower (stable) and spherical higher (quasistable) for $A\in[A_0,A_c]$, and vice versa for $A\in[A_c,A_1]$. This is a typical behavior in a discontinuous (first-order) phase transition, when the equilibrium jumps from one configuration to another at a certain ''critical'' value of a control parameter (the quotation marks used to avoid confusion with critical points such as the Curie temperature, etc.) and the two relevant phases coexist in a certain interval around. For $B=0$, however, all the above values coincide at $A_0=A_c=A_1=0$. In this γ-soft case, the $\beta_0\neq 0$ minimum coalesces with the $\beta_0=0$ minimum at $A=A_c$ and the corresponding transition is continuous (second order). By analyzing equilibrium solutions within the truncated geometrical model, we therefore clearly identify various types of phase-transitional behaviors; a schematic phase diagram is shown in Fig. 1(a).

In fact, the above-outlined phenomena are precisely those described within the classical Landau theory of phase transitions [39,40]. An analog of Eq. (3) can be written for any thermodynamic potential, where coefficients $A, B, C, \ldots$ depend on some external control parameters (thermodynamic variables) and β represents an order parameter, which characterizes the immediate state of the system (we now disregard γ). The order of a phase transition—according to the Ehrenfest classification [1]—is given by the lowest rank of the derivative of $V(\beta_0)$ with respect to the control parameters that changes discontinuously at the transitional point.

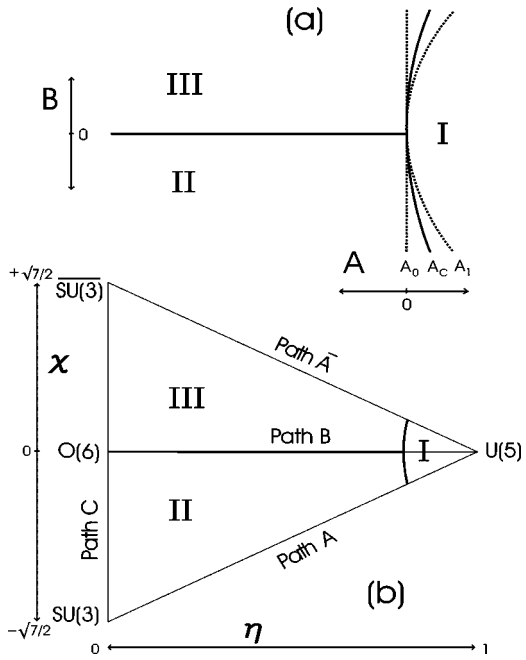

FIG. 1. (a) The shape-phase diagram of the GM potential (3). Phases I, II, and III correspond to spherical, prolate, and oblate axisymmetric shapes, respectively. (b) The shape-phase diagram (extended Casten triangle) of the IBM Hamiltonian (8) with the corresponding dynamical symmetries and transitional paths A–C.

Note that the Landau theory was for the first time explicitly applied to nuclear quadrupole shapes in the context of hot rotating nuclei—see Ref. [7], where the above results are already discussed.

According to the Landau theory [40], a continuous phase transition between $\beta_0=0$ and $\beta_0\neq 0$ equilibrium states can be located in the parameter space only at an intersection of three or more discontinuous phase transitions, the phase separating curves in the simplest case forming a ''T junction'' in the phase diagram. This is exactly what we observe in Fig. 1(a) since the $A=B=0$ second-order transition is a crossing of the spherical-prolate ($A=A_c$, $B<0$), spherical-oblate ($A=A_c$, $B<0$), and prolate-oblate ($B=0$, $A<0$) first-order transitions. Indeed, at the border between prolate and oblate shapes, $B=0$, the minimum $\beta_0>0$ flips to $-\beta_0$ in a discontinuous way, giving rise to the prolate-oblate first-order phase transition [24,31]. Let us note that the existence of this phase transition and the role of the continuous transition at $A=B=0$ as a ''triple point'' of the phase diagram in Fig. 1(a), in the sense of the Landau theory, was recognized only very recently [31,34].

If compared to other first-order phase transitions, the prolate-oblate transition has one exceptional feature: it has no finite interval of phase coexistence. When looking at potential (3), as it varies with B around the transition, one sees that it has a double-minimum form (with minima at β_0 and $-\beta_0$) for any B. However, we must not forget that γ in Eq. (3) can only be disregarded as far as the global minimum is concerned. With the γ dependence included, the upper minimum in β turns out to be only a saddle point and the whole $V(\beta,\gamma)$ has just one physical minimum, either $\beta_0>0$, $\gamma_0=0$, or $\beta_0<0$, $\gamma_0=0$ [this minimum is of course trivially repeated at $(\beta,\gamma)=(\beta_0,2\pi/3)$ and $(-\beta_0,\pi/3)$ due to the periodicity of the potential].

Depending on particular values of the constants A, B, and C, the height of the barrier separating two degenerated minima in the region of spherical-deformed phase coexistence at $A=A_c$ can be just few eV, much less than the ground-state average kinetic energy. Thus the potential may be considered practically flat in the transitional region. This recently led Iachello [28] to the concept of critical-point symmetries, which result from replacing of $V(\beta,\gamma)$ in the vicinity of $A=A_c$ by an infinite square well in β. As this could only be achieved with terms in Eq. (3) up to infinite order, the critical symmetries only approximate real eigensolutions of the collective Hamiltonian. On the other hand, a close realization of the analytic predictions based on this assumption in some nuclei [29] shows that the approximation is rather realistic.

It is evident that fluctuations due to the zero-point motion in a finite quantum case make realistic shape transitions smoother. Nevertheless, an abrupt change of the ground-state structure at $A=A_c$ can be observed if the kinetic-energy average for the ground state is much less than the depth of the deformed minimum. Another obstacle on the way to identify phase-transitional behavior in atomic nuclei is the fact that since real nuclei contain only an integer number of nucleons, nature does not allow us to vary the control parameters continuously in the region where the phase transition occurs. This leads to discrete changes in the properties of nuclei around the transition point, making an extension of the above concepts to systems with a limited number of constituents of general importance.

B. Interacting boson model

In contrast to the simplicity and universality of the above-outlined analysis, there is no ''geometry'' that could be directly extracted from the ultimately microscopic description of nuclei. This underlines the importance of algebraic approaches, the interacting boson model [36] being the most popular example. The IBM s and d bosons with angular momenta 0 and 2, respectively, have microscopic origin in nucleonic Cooper pairs and they equivalently describe quanta of collective excitations in an appropriate coordinate representation, allowing thus for a geometric interpretation. In particular, dynamical symmetries of the sd-IBM represent integrable forms of an anharmonic vibrator [spherical shape associated with the U(5) dynamical symmetry], an axisymmetric rotor [prolate or oblate shapes corresponding to SU(3) or $\overline{\mathrm{SU(3)}}$ symmetries, respectively], or a γ-soft rotor [both O(6) and $\overline{\mathrm{O(6)}}$ dynamical symmetries].

The geometric content of the sd-IBM is derived using condensate states [10,11,41,42],

$$|N,\beta,\gamma\rangle=\frac{1}{\sqrt{\mathcal{N}}}\left(s^\dagger+\beta\cos\gamma d_0^\dagger+\frac{\beta\sin\gamma}{\sqrt{2}}[d_{-2}^\dagger+d_{+2}^\dagger]\right)^N|0\rangle, \tag{5}$$

where $|0\rangle$ is the boson vacuum, $s^\dagger$ and $d_\mu^\dagger$ create bosons of

the respective types (μ is the angular-momentum projection), and $\mathcal{N}=N!(1+\beta^2)^N$ ensures the normalization to unity. N represents the total boson number, a finite and conserved quantity in the IBM, which forms the most important difference from geometric collective models. Coefficients β and γ are given the same interpretation as those in Eq. (3), i.e., deformation parameters in the intrinsic frame. States (5) are used as trial wave functions for the variational procedure, estimating the energy and wave function of the IBM ground state for a Hamiltonian H by minimization of $\langle H\rangle = \langle N,\beta,\gamma|H|N,\beta,\gamma\rangle$ with respect to β and γ.

To assure appropriate scaling with variable N, the IBM energy is calculated per one boson, $\mathcal{E}=\langle H\rangle/N$, and one gets a general expression

$$\mathcal{E}(\beta,\gamma)=\frac{A\beta^2+B\beta^3\cos 3\gamma+C\beta^4}{(1+\beta^2)^2}, \tag{6}$$

where A, B, and C depend on the particular Hamiltonian H under study [43]. Note that Eq. (6) is exactly of form (3), with the higher-order terms given by an expansion of $(1+\beta^2)^{-2}$. The denominator is important since it makes the $\beta\to\infty$ asymptotics of $\mathcal{E}$ finite, equal to C, in agreement with finite bounds of IBM energy spectra. Although H is the full Hamiltonian, the resulting energy functional represents in fact a ''potential'' similar to that in Eq. (3). This is so since the condensate states (5) carry zero linear momentum and the kinetic terms, therefore, do not contribute to $\langle H\rangle$. A related procedure [44] using time-dependent variational principle with Glauber coherent states yields both kinetic and potential terms, the latter converging to the condensate value for $N\to\infty$. This represents the classical limit of the system, in which the zero-point motion vanishes and the condensate states become exact and orthonormal eigenstates of the Hamiltonian.

The shape-phase analysis based on Eq. (6) is analogous to that of Eq. (3). One can identify transitions between spherical and deformed shapes in the same way as before, yielding the same critical value (4). The phase coexistence interval is again bounded by $A_0=0$ from below, but the upper bound A_1 is given by a more complicated condition than before since for Eq. (6) it follows from a cubic equation, in contrast to the previous quadratic case. The γ-soft $B=0$ line for $A<0$ again represents the first-order phase transition between prolate and oblate geometries. In this way the O(6) dynamical symmetry becomes an exact critical-point symmetry of the IBM [31,32].

Note that while the spherical-deformed nuclear shape-phase transitions, both continuous and discontinuous, have been discussed in the IBM context already since 1980 [10], the prolate-oblate transition with all its consequences remained unrecognized until very recently [24,31–34]. This is certainly connected with the long-persistent belief that the prolate-oblate transformation within the IBM is only due to an unimportant gauge transformation, induced by a change of the relative phase between s and d bosons [36,45]. This transformation is a special case of a discrete, parameter symmetry [46,47] that links isospectral pairs of IBM Hamiltonians $H(\vec{\lambda})$ and $H(\vec{\lambda}')$ corresponding to prolate and oblate deformations through a unitary similarity transformation: $H(\vec{\lambda}')=U(\vec{\lambda}',\vec{\lambda})\,H(\vec{\lambda})\,U^{-1}(\vec{\lambda}',\vec{\lambda})$. Since this operation changes the sign of B in Eq. (6), the prolate-oblate transition $\beta_0\mapsto-\beta_0$ at $B=0$ could be seen just as a mirrorlike symmetry and not a real phase transition. However, we stress that the energy spectra are not constituents for the phase-transitional behavior, in contrast to the structure of eigenstates. Regardless of the parameter symmetry, the prolate/oblate isospectral Hamiltonians represent incompatible modes of motion, so that the essential condition in Eq. (2) is fulfilled. In fact, the prolate-oblate transition can proceed along a path $\vec{\lambda}=\vec{\lambda}(t)$ such that the spectra are not symmetric around the transitional point t_c, but the ground-state wave function still exhibits the characteristic jump at this point.

It should be pointed out that the IBM phase transitions can rigorously be studied only in the limit of an infinite boson number N, which is completely unrealistic when applied to nuclei. Although the general form (6) is valid for any finite N, only in the classical limit the condensate trial wave functions (5) become exact and the above-discussed jumps of the control parameter actually take place. Nevertheless, it has been shown (and will also follow from the present work) that even in finite-N cases the characteristic signatures of changing structures are observed, despite the fact that the finite-size effects tend to wash out the phase-transitional behavior [20].

In this context it becomes interesting to compare the above results with those following from an extension of the condensate variational method by projecting the trial states to zero angular momentum [48]. Indeed, although the average projection of the IBM angular momentum $L=\sqrt{10}[d^\dagger\times\tilde{d}]^{(1)}$ to any direction is zero for states (5), the average of L^2 does not vanish, which is of course unrealistic for the 0^+ ground state. The $L^2=0$ projected method represents better approximation of the ground-state behavior for any finite N. It leads, however, to the losts of phase transitions in the finite-N cases, since the minimum of the generalized energy functional (obtained by a numerical calculation) moves continuously with varying η and χ [26]. For $N\to\infty$, naturally, the projected results converge to the present ones, including of course all phase-transitional effects discussed above. This agrees with the general understanding that real critical behaviors can apply only to infinite systems.

C. Semimicroscopic models

As pointed out above, the IBM is believed to represent an approach somewhere in between the purely phenomenological geometric model and a microscopically based fermion model. It is clear that on the way from microscopic to the IBM description one must deal with the problem of mapping the real fermion pairs, which regardless of carrying some bosonic features still obey restrictions given by the Pauli principle, onto the true s and d bosons of the IBM. Although this problem—in spite of large amount of effort spent on it up to now—cannot be declared as solved so far, a lot of insight into the microscopic foundations of nuclear boson

models has already been gained [49]. The fermion models that seem to get closest to the IBM are the Ginocchio model [50] and the subsequent fermion dynamical-symmetry model (FDSM) [51]. The correspondence between states of these models and states of the IBM was studied in detail, as well as the mapping of relevant physical fermion operators into the s,d-boson space [49,52].

In both of the above-mentioned fermion models, the idea [50] of splitting the total single-nucleon angular momentum into pseudo-orbital and pseudospin components is utilized. The angular momentum 0 or 2 of nucleonic S and D pairs, respectively, is given by coupling only the so-called active components (either the pseudo-orbital or pseudospin ones), the other (inert) components being coupled to zero. In the case of the pseudospin active components, the Ginocchio SO(8) model is obtained [50,51], while the pseudo-orbital active components lead to the FDSM with the Sp(6) dynamical algebra [51]. Both of these possibilities result in an algebraic description and make it possible to exploit the generalized coherent states [41]

$$|\eta\rangle = R_{\rm int}(\eta)\exp\left(\eta_{00}S^{\dagger} + \sum_{\mu}\eta_{2\mu}D^{\dagger}_{\mu} - \text{H.c.}\right)|0\rangle, \quad (7)$$

to extract the corresponding geometry [13,14]. Indeed, although general $\eta \equiv \eta_{\lambda\mu}$ in Eq. (7) contain 12 real parameters, the transformation $R_{\rm int}(\eta)$ to the intrinsic frame [13,14] ensures that the resulting energy functional $\langle H_{\rm F}\rangle = \langle \eta|H_{\rm F}|\eta\rangle$ (where $H_{\rm F}$ is a fermionic Hamiltonian) depends just on the Hill-Wheeler coordinates β and γ.

The analysis in the SO(8) case [13] leads to γ-soft shapes while, on the other hand, the Sp(6) FDSM results in γ-rigid quadrupole shapes [14]. This again implies first- or second-order phase transitions—in the γ-rigid or soft cases, respectively—between spherical and deformed shapes. With the fermionic Hamiltonian containing at most two-body terms, the energy functional has the general form (3), allowing for both axially symmetric prolate ($\beta_0 > 0,\ \gamma_0 = 0$) and oblate ($\beta_0 < 0,\ \gamma_0 = 0$) equilibrium solutions. In addition, Pauli blocking effects restrict the available region in the $\beta \times \gamma$ plane, which under some conditions on the particle number leads to the onset of triaxiality [14] [Eq. (3) cannot be minimized in the whole plane]. This results in additional (second-order) phase transitions that were missing in the simpler geometric and interacting boson models.

The particle number—and not only the interaction strengths in $H_{\rm F}$—in fact becomes the principal control parameter for the phase transitions between various shape types in both the SO(8) and Sp(6) cases. This of course fully conforms with the shared understanding of the nature of nuclear ground-state shape-phase transitions, since the varying number of nucleons is not expected to produce rapid changes of strengths in the microscopic Hamiltonian, so that the particle number alone must be responsible for majority of transitional effects. It also turns out [13,14] that the transition from deformed to spherical shapes is related to an abrupt change of pairing properties, indicating that while the spherical phase is associated with strong pairing correlations, in the deformed phase these correlations become much looser (see also Ref. [53]). This conclusion was recently invoked to interpret results of an extended phase-transitional analysis of the IBM with cranking [35], where the rotation-induced transition from spherical to deformed phase closely resembles behaviors observed in systems with competing superconducting and normal phases.

An interesting feature of the SO(8) model is that the phase transition between spherical and deformed γ-soft shapes is connected with a special dynamical symmetry of the model, SO(7). This appears to be a ''critical dynamical symmetry'' characterized by β-soft shapes of the potential well, in complete analogy with much later analysis [28] of ''critical-point symmetries'' in the framework of the geometric model (see Sec. II A). Let us stress that SO(7) is an exact dynamical symmetry of the Ginocchio model and at the same time a critical-point symmetry for the spherical-deformed γ-soft transition, which may be compared to the recently discovered double role of the exact O(6) dynamical symmetry in the IBM [31,32] (the latter, however, being related to the transition between prolate and oblate shapes, see Sec. II B). Based on the mapping of the SO(8) model onto the IBM [52] it was shown [54] that the SO(7) critical-point symmetry corresponds to the U(5) dynamical symmetry of the IBM with, however, a modified choice of operators (non-Hermitian) of electromagnetic transitions.

It is clear that a comprehensible discussion of problems outlined in this section would require much more space than available in the present paper. The main aim of this review was to illustrate the rich variety of aspects that should be integrated in a comprehensible theory of shape-phase transitions in nuclei, a theory we still only start developing. In the rest of this paper we focus on phase-transitional properties of the interacting boson model.

III. SPECTROSCOPIC SIGNATURES OF SHAPE-PHASE TRANSITIONS

A. Extended Casten triangle

We use the well-known two-parameter IBM Hamiltonian

$$H(N,\eta,\chi) = \eta n_d - \frac{1-\eta}{N}Q(\chi)\cdot Q(\chi) \quad (8)$$

with the control parameters changing in the range $\eta \in [0,1]$ and $\chi \in [-\sqrt{7}/2, +\sqrt{7}/2]$. Here $n_d = d^{\dagger}\cdot\tilde{d}$ is the d-boson number operator and $Q(\chi)$ the quadrupole operator,

$$Q(\chi) = d^{\dagger}s + s^{\dagger}\tilde{d} + \chi[d^{\dagger}\times\tilde{d}]^{(2)}. \quad (9)$$

As we consider the parameters η and χ to be dimensionless, Eq. (8) needs to be multiplied by an arbitrary factor defining the actual energy scale. The $\eta\times\chi$ parameter plane can be naturally represented by an extended Casten triangle in Fig. 1(b) [31,32] where the $\chi = \text{const}$ coordinate lines are assumed to all intersect in the $\eta = 1$ vertex. This vertex corresponds to the U(5) dynamical symmetry, the others to the SU(3) and $\overline{\text{SU(3)}}$ symmetries, at $(\eta,\chi) = (0, -\sqrt{7}/2)$ and $(0, +\sqrt{7}/2)$, respectively. The O(6) symmetry is located at $\eta = \chi = 0$, i.e., in between the SU(3) and $\overline{\text{SU(3)}}$ vertices.

Compared with the standard Casten triangle, whose vertices were the standard dynamical symmetries U(5), SU(3) (prolate), and O(6), the extended triangle is doubled to include also the oblate shapes.

The above-discussed prolate-oblate parameter symmetry [46,47] connects a given point (η,χ) with its mirror image $(\eta,-\chi)$. It means that the added half of the triangle contains Hamiltonians that are isospectral with those in the standard triangle. Note that we use the consistent-Q formalism, in which the quadrupole operator (9) in the Hamiltonian (8) coincides with the quadrupole operator used to determine the strengths of quadrupole transitions and average quadrupole moments. In this case, the mirror reflection of χ in the Hamiltonian produces also the sign change of the quadrupole moments associated with individual eigenstates, in agreement with the geometric interpretation of the associated parameter symmetry. The additional parameter symmetry along the O(6)–U(5) transition, as discussed in Ref. [46], leads outside the given parameter range: it would form a leg pointing out of the plane from the U(5) vertex to $\overline{\mathrm{O}(6)}$, but we do not consider this transitional line here. In any case, parametrization (8) does only span a two-dimensional plane in the six-dimensional parameter space of the general IBM, but one that is extremely rich in structures.

The shape analysis of the Hamiltonian (8) using the condensate-state method leads to the energy functional (6) with coefficients in the $N\to\infty$ limit given by the following expressions [20,34,43]:

$$A_\infty(\eta)=5\eta-4, \tag{10}$$

$$B_\infty(\eta,\chi)=4\sqrt{\frac{2}{7}}\chi(1-\eta), \tag{11}$$

$$C_\infty(\eta,\chi)=\eta-\frac{2}{7}\chi^2(1-\eta). \tag{12}$$

This conforms with the standard geometric interpretation of the IBM dynamical symmetries and yields the phase diagram of the Hamiltonian (8), as schematically shown in Fig. 1(b): the phase separatrix between deformed prolate ($\chi<0$) and oblate ($\chi>0$) shapes is the $\chi=0$ line for $\eta<4/5$, while the separatrix between deformed ($\eta<\eta_c$) and spherical ($\eta>\eta_c$) shapes is given by

$$\eta_c=\frac{4+2\chi^2/7}{5+2\chi^2/7} \tag{13}$$

for both prolate and oblate shapes and $N\to\infty$. Note that with the N-dependent interaction coefficient in Eq. (8), which ensures the appropriate relative scaling of both terms for variable boson number, finite-N effects in Eq. (13) are given just by a quickly vanishing additive term $O(N^{-1})$. At the intersection of the two above curves of discontinuous phase transitions, at $(\eta,\chi)=(4/5,0)$, the transitions become continuous [34].

Below we will analyze the behavior of various observables along several transitional paths between limiting dynamical symmetries. Although one can consider also more general possibilities [20], the paths will be realized here simply by fixing one of the parameters in the Hamiltonian (8) and varying the other—see Fig. 1(b).

Path A: $\chi=-\sqrt{7}/2$, *variable* η. The Hamiltonians along this leg of the Casten triangle interpolate between the SU(3) and U(5) symmetries and contain no admixtures of the $\mathcal{C}_2[\mathrm{O}(6)]$ and $\mathcal{C}_2[\mathrm{O}(5)]$ Casimir operators. According to Eq. (13), the first-order phase transition between prolate and spherical geometries takes place at $\eta=9/11=0.818\,18\ldots$ (for $N\to\infty$).

Path $\overline{\mathrm{A}}$: $\chi=+\sqrt{7}/2$, *variable* η. This path is a mirror image of path A and represents the $\overline{\mathrm{SU}(3)}$-U(5) (oblate-spherical) transition. We will not separately consider this path since due to the parameter symmetry all the results are either identical with those for Path A or can be trivially deduced from them.

Path B: $\chi=0$, *variable* η. This is the O(6)-U(5) transitional path corresponding entirely to γ-soft shapes. The Hamiltonians here contain no admixtures of the SU(3) and $\overline{\mathrm{SU}(3)}$ invariants. The second-order phase transition between deformed and spherical shapes is located at $\eta=4/5=0.8$, which is also a triple point of shape phases in the extended Casten triangle.

Path C: $\eta=0$, *variable* χ. These Hamiltonians are transitional between the SU(3) and $\overline{\mathrm{SU}(3)}$ dynamical symmetries, with the O(6) symmetry in the middle. The O(6) point is a phase transition between prolate and oblate shapes and the central point of the $\chi\leftrightarrow-\chi$ parameter symmetry. It should be noted that the Hamiltonians along this path—if decomposed into a linear combination of Casimir invariants corresponding to the standard U(5), O(6), O(5), SU(3), and O(3) symmetries—contain nonvanishing components of the U(5) invariants (except, of course, at $\chi=0$ and $-\sqrt{7}/2$) but these can be avoided if the $\mathcal{C}_2[\overline{\mathrm{SU}(3)}]$ Casimir operator is included into the decomposition.

For paths A, $\overline{\mathrm{A}}$, and B, the Hamiltonian (8) is apparently of the linear form (1) with

$$H_0=-\frac{1}{N}Q(\chi)\cdot Q(\chi),$$

$$V=n_d-H_0 \tag{14}$$

(and, of course, $\lambda\equiv\eta$). For path C, however, the dependence on χ is clearly quadratic. Nevertheless, if only a small interval of χ is considered, the linearization can be done approximately [32]. For instance, near the phase transition at $\chi=0$ one can neglect the terms with χ^2 and again obtain Eq. (1) with

$$H_0=-\frac{1}{N}Q(0)\cdot Q(0),$$

$$V=-\frac{2}{N}(s^\dagger\tilde{d}+d^\dagger s)\cdot(d^\dagger\tilde{d})^{(2)} \tag{15}$$

(for $\lambda\equiv\chi$).

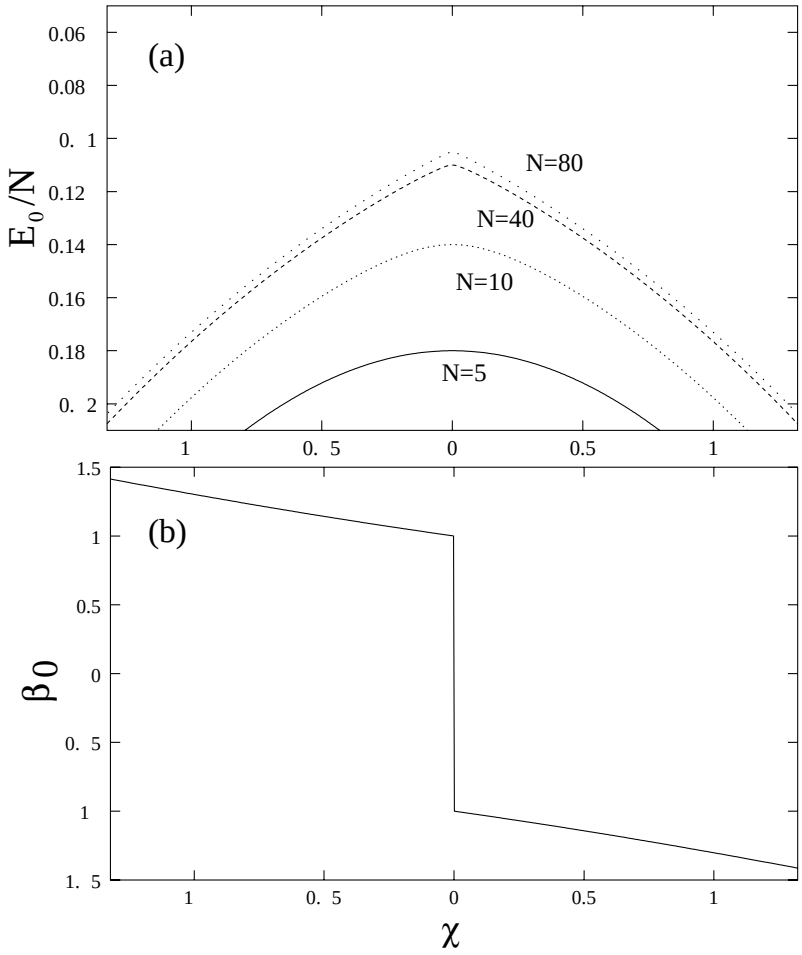

FIG. 2. The ground-state energy per boson [panel (a)] for the Hamiltonian (8) with $N=5-80$, and the location of the potential minimum β_0 [panel (b)] along path C.

B. Phase-transitional observables

In this section, we discuss some observables suitable for detecting the phase-transitional behavior and also for locating nuclei near transitions in the extended Casten triangle. It should be stressed that many such observables have already been studied before, mainly for the SU(3)-U(5) transition (path A) [10,20,21,25–27,30,33], but also for the O(6)-U(5) (path B) [10,30,33] and recently for SU(3)-O(6)-$\overline{\mathrm{SU(3)}}$ transitions (path C) [31,32]. We will now generalize these studies to the whole extended triangle and investigate the dependence on the number of bosons. The way we adopted to systematically study these issues relies on using IBM calculations with boson numbers varying from small to large values (up to $N=80$). This makes it possible to single-out observables and effects related to phase transitions, determine their N dependence, and apply these findings in the low-N limit to study empirical nuclei. Note that the discussion of finite-N effects will continue from various viewpoints also in the forthcoming sections.

To illustrate a typical phase-transitional behavior, let us first consider the Hamiltonian (8) along the prolate-oblate transitional path C. This transition was discussed recently both from the theoretical and experimental viewpoints [31,32]. In Fig. 2(a) we show the absolute energy per boson of the 0^+ ground state for 5, 10, 40, and 80 bosons. The curves for increasing N must converge to that for $N\rightarrow\infty$, given by the minimal value of the energy functional in Eq. (6) with Eqs. (10)–(12) ($\eta=0$). At the phase transition, $\chi=0$, the ground-state energy makes a kink of which the sharpness increases with N. In the asymptotic limit, the tangent becomes really discontinuous, as follows from the first-order transitional behavior illustrated in Fig. 2(b) by the flip of β_0. In the present parametrization of the Hamiltonian, the ground-state energy is symmetric with respect to the transitional point due to the $\chi\leftrightarrow-\chi$ parameter symmetry. Note, however, that this mirrorlike symmetry could be avoided—without affecting the phase-transitional behavior—if the Hamiltonian (8) is extended by another term, for instance, the SO(3) invariant with a χ-dependent weight.

To show that the prolate-oblate transition represents an irreducible transitional class, regardless of the parameter symmetry, let us consider the SU(3) wave-function entropy of the ground state. This quantity is independent of possible admixtures of the SO(3) invariant. The wave-function entropy [55,56]

$$W_0^{\mathcal{B}}=-\sum_i |\langle\Psi_0|i^{\mathcal{B}}\rangle|^2\ln|\langle\Psi_0|i^{\mathcal{B}}\rangle|^2 \qquad (16)$$

measures the fragmentation of the ground-state wave function $|\Psi_0\rangle$ in the eigenbasis $\mathcal{B}\equiv\{|i^{\mathcal{B}}\rangle\}$ corresponding to the given dynamical symmetry, SU(3) in the present case. In Fig.

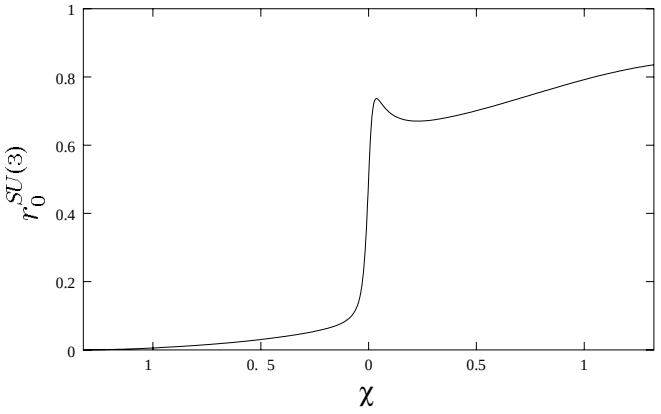

FIG. 3. SU(3) wave-function entropy ratio along path C for $N=30$.

3 the quantity $r_0^{\mathrm{SU}(3)}=(\exp W_0^{\mathrm{SU}(3)}-1)/r_{\mathrm{GOE}}$, as introduced in Ref. [56], is shown for path C to demonstrate a nontrivial dependence of the SU(3) entropy on χ (no mirrorlike symmetry is observed). In fact, the denominator r_{GOE} ensures that $r_0^{\mathcal{B}}\approx 1$ if the ground state has a completely random overlap with $\mathcal{B}$, while clearly $r_0^{\mathcal{B}}=0$ for the ground-state identical with one of the basis vectors. Since Fig. 3 shows an abrupt change from $r_0^{\mathrm{SU}(3)}\approx 0$ to ≈ 0.8 at $\chi\approx 0$, it is clear that the intermediate-χ ground state virtually coincides with the SU(3) ground state for $\chi<0$, but it suddenly becomes almost totally delocalized in the SU(3) eigenbasis at the critical point. Note that this effect, as discussed later, is due to the mixing of the ground state with the other 0^+ states, mainly with its nearest neighbor 0_2^+. It should also be pointed out that, in the present case, the $\overline{\mathrm{SU}(3)}$ wave-function entropy would have exactly opposite behavior.

We now turn to characteristic observables indicating structural changes in nuclei around the shape-phase transitions across the whole extended Casten triangle. Still one of the clearest experimental signatures traditionally used to identify such changes is the two-nucleon separation energy [10,30]. This quantity can be extracted from the absolute ground-state energies (masses) of neighboring even-even nuclei and is therefore predictable also from the IBM, provided one knows how the IBM parameters depend on the nuclear mass number. In Fig. 4 we have plotted the ground-state energy per boson for the whole triangle for $N=10$ and 80. As exemplified by the $N=10$ case, the ground-state energy for lower boson numbers shows a much smoother behavior than the $N\to\infty$ limit, but still the transitional effects can be experimentally detected [30].

Other signatures of nuclear shape-phase transitions concern spectra and quantum characteristics of low-lying collective states and the associated transition rates [23,25–29,31–33]. Although these quantities are not literally properties of the ground state, they are intimately connected with the ground-state phase transitional behavior. We will demonstrate here variations of a few selected quantities, namely, the ratio of excitation energies for the first excited 4^+ and 2^+ states, $R_{4/2}$, the quadrupole moment of the first excited 2^+ state, $Q(2_1^+)$, and a rate of the electric quadrupole transition

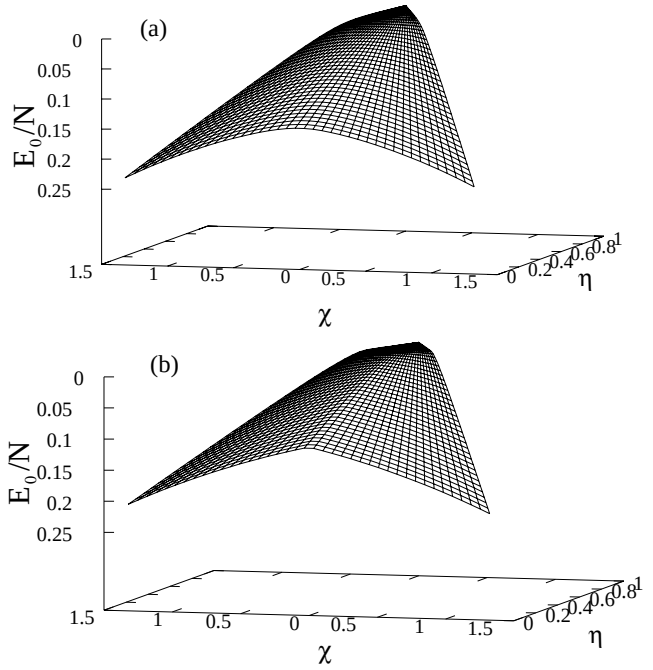

FIG. 4. The ground-state energy per boson across the extended Casten triangle for $N=10$ (a) and 80 (b).

between second and first excited 2^+ states, $B(E2;2_2^+\to 2_1^+)$. Each of these signatures reveals important structural information: The value of $R_{4/2}$ is 3.33 for SU(3) and $\overline{\mathrm{SU}(3)}$-like nuclei, around 2.5 for O(6)-like nuclei, and around 2 for U(5)-like nuclei. The quadrupole moment, which is directly related to the equilibrium value β_0, allows to observe the prolate-oblate transition: $Q(2_1^+)$ is negative for prolate, positive for oblate, and zero for γ-soft nuclei (we are dealing now with the laboratory quadrupole moment, in contrast to the intrinsic one reflected by β_0; this explains the sign inversion). $B(E2;2_2^+\to 2_1^+)$ is zero in the SU(3) and $\overline{\mathrm{SU}(3)}$ limits, but nonzero everywhere else; it essentially measures whether the O(5) symmetry is present. These signatures are shown across the whole extended triangle in Fig. 5 for $N=5$ (upper row) and 40 (lower row). The location of the phase transitions is clearly indicated by sharply varying observables. The N dependence shows that for realistic boson numbers, $N\approx 5$–10, the signatures behave smoother than for higher values, but they still can be used to unambiguously locate a given nucleus in the transitional region. They have been applied in the Hf-Hg mass region [31,32], related to the above example with $\eta=0$.

C. Thermodynamic and Coulomb-gas analogies

We saw in Figs. 2 and 4 that the change of the ground-state energy at the critical points becomes sharper with increasing boson numbers. A very sensitive probe of the phase-transitional behavior is the second derivatives of the ground-state energy (per boson) with respect to the control parameters:

$$c(\lambda_i)|_{\{\lambda_j\}}=-\frac{\partial^2}{\partial\lambda_i^2}\mathcal{E}_0(\vec{\lambda}) \tag{17}$$

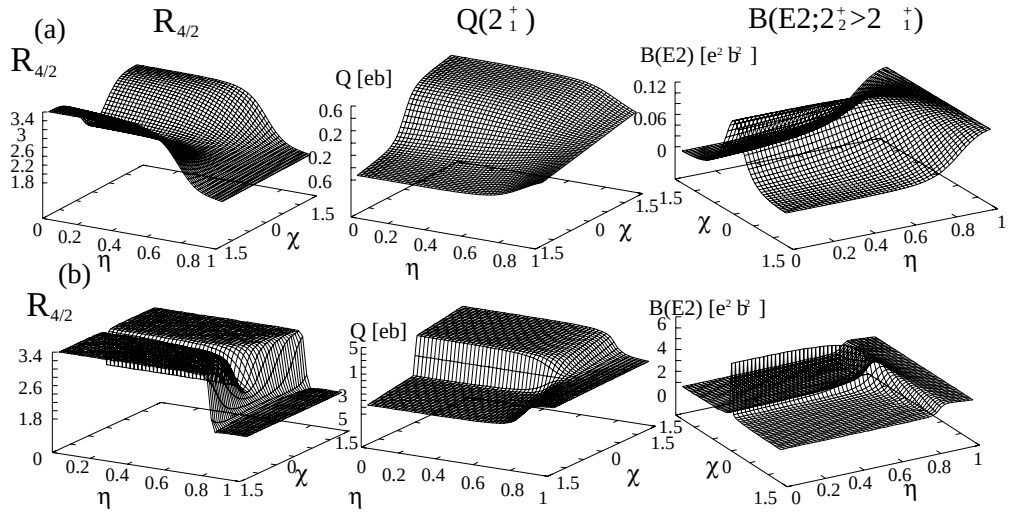

FIG. 5. The observables $R_{4/2}$, $Q(2_1^+)$, and $B(E2;2_2^+ \rightarrow 2_1^+)$ across the extended Casten triangle for $N=5$ [row (a)] and 40 [row (b)].

(where all λ_j's with $j \neq i$ are kept constant). These are shown for the three transitional paths—A/$\overline{\text{A}}$, B, and C—in panels (a) of Figs. 6, 7, and 8, respectively. In the above-discussed thermodynamic analogy, $\mathcal{E}_0(\vec{\lambda})$ is replaced by the equilibrium value of the thermodynamic potential, $F_0(p,T)$ (where p and T are pressure and temperature). Its second derivative with respect to temperature determines the specific heat (or heat capacity) of the system, $c(T)|_p = -T\partial^2 F_0(p,T)/\partial T^2$,

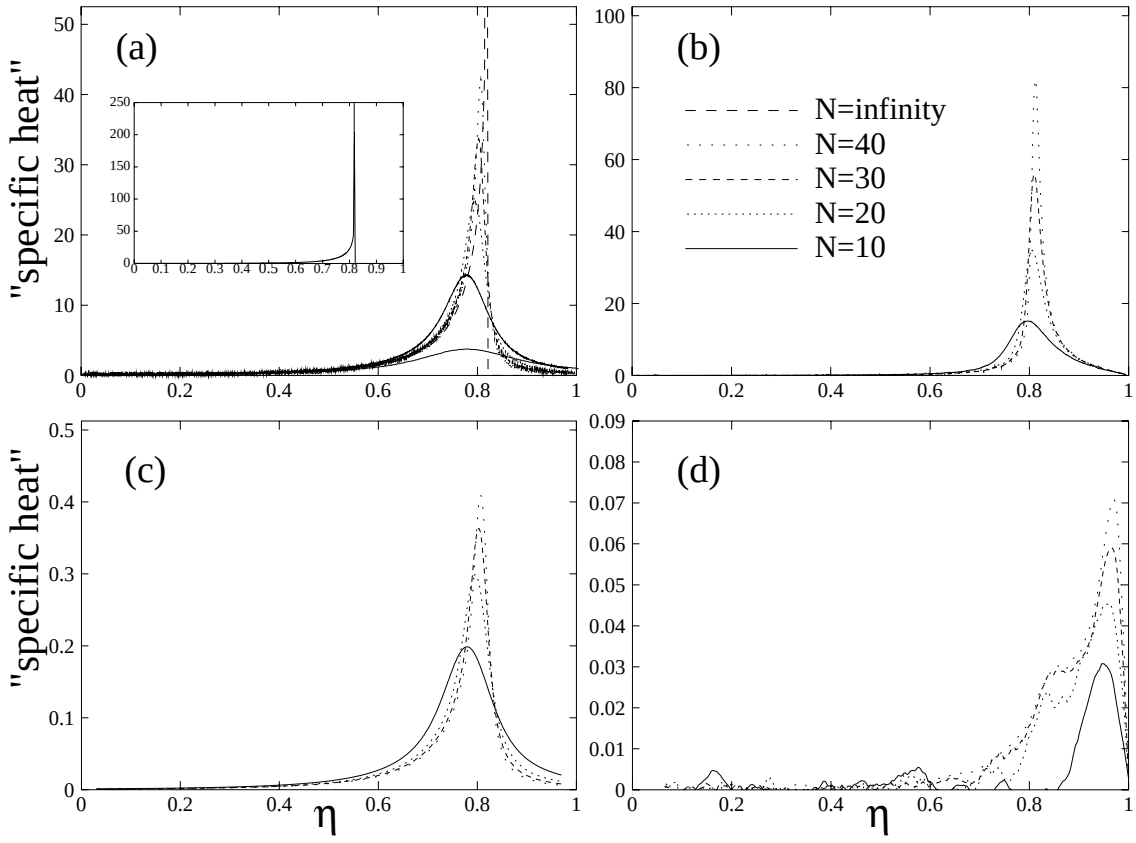

FIG. 6. The ''specific heat'' of the ground state for paths A and $\overline{\text{A}}$ calculated following four definitions discussed in the text: (a) from the second derivative of the ground-state energy, $c(\eta)$ according to Eq. (17), (b) from the first derivative of the U(5) wave-function entropy, $c'(\eta)$ in Eq. (18), (c) from thermal properties of the randomized IBM, $c_{\text{th}}(\eta)$ in Eq. (23), and (d) from the first derivative of the U(5) overlap entropy, $c'_{\text{th}}(\eta)$ in Eq. (26). In all cases, the η dependence of the ''specific heat'' is shown for boson numbers from 10 to 40; the asymptotic limit (in the full scale shown in the inset) and the $N=5$ dependence (the lowest curve) are given for (a).

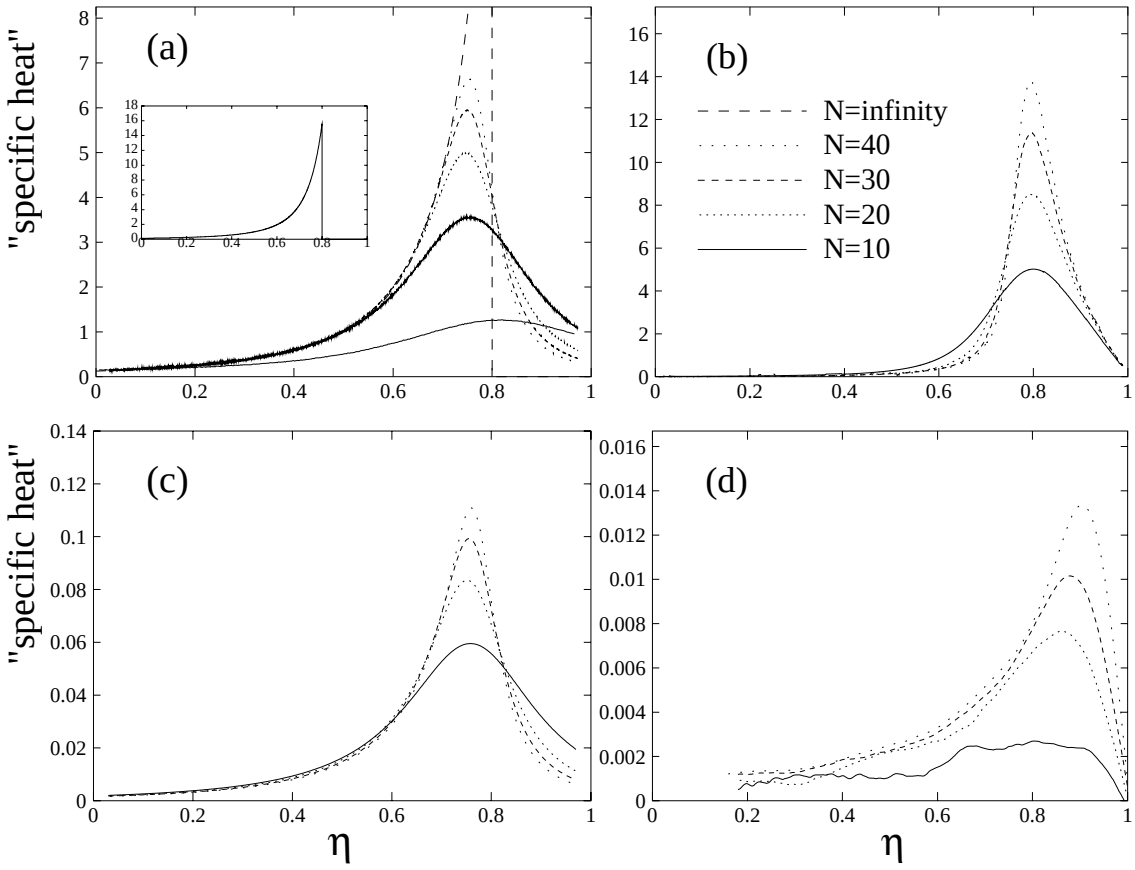

FIG. 7. The same as in Fig. 6, but for path B.

whereas the second derivative with respect to pressure yields the compressibility, $c(p)|_T = -V^{-1}\partial^2 F_0(p,T)/\partial p^2$ [40]. Inspired by the first of these terms, we will call both of the quantities $c(\eta)|_\chi = -\partial^2 \mathcal{E}_0(\eta,\chi)/\partial\eta^2$ and $c(\chi)|_\eta = -\partial^2 \mathcal{E}_0(\eta,\chi)/\partial\chi^2$ the "specific heat."

It can be seen in panel (a) of Figs. 6–8 that the "specific heats" derived from the second derivatives of the ground-state energy have maxima in the critical regions. As expected, the sharpness of these peaks increases with an increasing boson number, the maximum moving towards the η_c value (for lower N, the critical η is shifted due to finite-N corrections of the coefficients A, B, and C, cf. Refs. [20,34]). The curve corresponding to the asymptotic limit $N\to\infty$, as determined from the energy functional in Eqs. (6) and (10)–(12), is also shown for the paths A/$\overline{\text{A}}$ and B. It has a singular behavior for the first-order phase transition on paths A/$\overline{\text{A}}$, see Fig. 6(a) (also on path C), while it is only discontinuous for the second-order phase transition on path B, see Fig. 7(a). Clearly, the finite-N curves converge to the asymptotic limit but even the $N=40$ case is still far away from it, indicating that the second derivatives considered here are indeed a very powerful magnifying glass.

In the above thermodynamic analogy, the first derivative of the ground-state energy with respect to the control parameter determines an analog of entropy [in the thermodynamic case we have $S=-\partial F_0(p,T)/\partial T$]. As follows from the peaked form of the "specific heat," the entropy has a steplike behavior at the phase-transitional point. There is, however, another entropic quantity that behaves in a similar way and could thus be used to determine an alternative "specific heat" in the present case. It is the wave-function entropy of the ground state in an appropriate dynamical-symmetry basis [20,26,56]. The wave-function entropy is defined by Eq. (16), where now the basis $\mathcal{B}$ will be the U(5) eigenbasis for paths A/$\overline{\text{A}}$ and B, and the SU(3) eigenbasis for path C. [Note that while path C could be equivalently characterized by the $\overline{\text{SU(3)}}$ entropy, the use of the SU(3) or $\overline{\text{SU(3)}}$ entropies for path A or $\overline{\text{A}}$, respectively, would be inconvenient since in the spherical-to-deformed transition the ground state does not flip to the SU(3) form instantly at the phase-transitional point. For the same reason, we do not use the O(6) entropy along path B.] We can thus define

$$c'(\lambda_i)|_{\{\lambda_j\}} = \mp\frac{\partial}{\partial\lambda_i} W_0^{\mathcal{B}}(\vec{\lambda}), \tag{18}$$

where we conveniently redefine the sign ($-$ for paths A/$\overline{\text{A}}$ and B, $+$ for C) to obtain similar behaviors as in panel (a) of Figs. 6–8. [We skip here any coefficient carrying suitable dimension of the "specific heat" in Eq. (18).] Indeed, panels (b) of Figs. 6–8 show the "heat capacity" (18) based on the U(5) or SU(3) wave-function entropies of the ground state for the respective paths. In all cases one again observes a sharpening of the phase-transitional peak with increasing N,

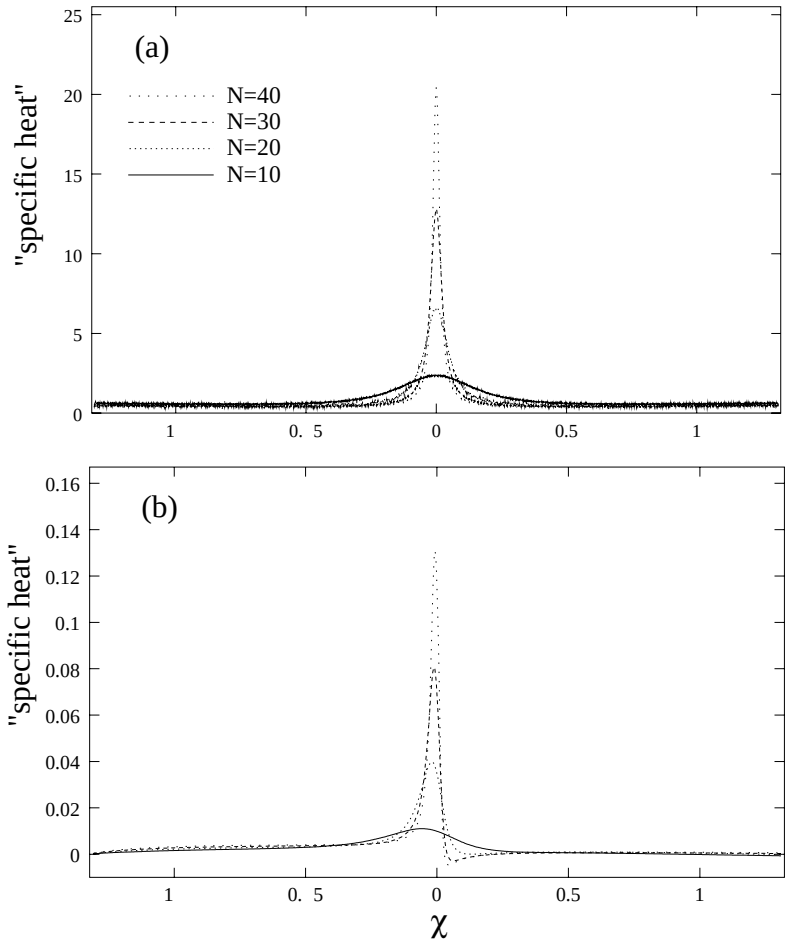

FIG. 8. Similar as in Fig. 6, but for path C. Because of the nonlinear dependence of the Hamiltonian on χ, only the cases analogous to (a) and (b) from Fig. 6 are relevant, where (a) is $c(\chi)$ according to Eq. (17) and (b) is $c'(\chi)$ determined from the χ derivative of the SU(3) wave-function entropy, Eq. (18).

which indicates a convergence of the corresponding wave-function entropy curve to its asymptotic steplike form.

If the dependence of the Hamiltonian on the varying control parameter is linear, as is the case for paths A/$\overline{\text{A}}$ and B, one can look at the phase-transitional behavior also from a completely different viewpoint. The new interpretation follows from the so-called Coulomb-gas analogy [57,58]: It is known that energy levels of the Hamiltonian (1) behave as a linear chain of charged particles on a plane interacting via Coulomb forces, the charges being determined by matrix elements of V. The control parameter λ plays a role of time, so that the second derivative $d^2E_0(\lambda)/d\lambda^2$ (where E_0 is the ground-state energy) is nothing but a force experienced by the ''particle'' corresponding to the ground state—the force from all the other particles that represent excited levels with the same spin and parity. In particular, one has [57]

$$c(\lambda)=2\sum_{i\neq 0}\frac{|\langle\Psi_i(\lambda)|V|\Psi_0(\lambda)\rangle|^2}{E_i(\lambda)-E_0(\lambda)}, \tag{19}$$

where $E_i(\lambda)$ is the ith energy of the Hamiltonian (1) and $|\Psi_i(\lambda)\rangle$ is the corresponding eigenvector. This expression can be applied to $c(\eta)|_\chi$ with $\chi=$const and η variable, since the Hamiltonian (8) depends on η linearly, see Eq. (14), but also to $c(\chi)|_\eta$ with $\eta=$const and χ variable for χ close to zero, where the linearization of the Hamiltonian [Eq. (15) generalized to $\eta\neq 0$] is locally valid.

The $N\to\infty$ behavior of $c(\eta)|_\chi$ or $c(\chi)|_\eta$ for paths A/$\overline{\text{A}}$–C in panel (a) of Figs. 6–8 indicates that the ground state gets a ''kick'' at the phase-transitional points. The force exhibits either a singularity (for paths A/$\overline{\text{A}}$ and C) or just a discontinuity (for path B), resulting in the respective first- or second-order phase-transitional behavior. The corresponding ''motion'' or '' trajectory,'' as given by the evolution of the ground-state energy, abruptly changes the direction (cf. Fig. 2), as in a hard-wall scattering, or just changes a ''rate of changing the direction.'' Naturally, the prominent role in sum (19)—just because of the denominator's increase with distance—has the terms corresponding to the closest levels, in particular to the first excited 0^+ state in our case. Nevertheless, more distant states can also bring considerable contributions if their ''charges,'' i.e., matrix elements in the numerator of Eq. (19), are large.

The level dynamics is tightly interrelated with the mixing properties of the eigenstate wave functions. The rate of mixing of the ground state for the linear Hamiltonian (1) with the ith excited state at a given λ can be represented by the quantity $M_i(\lambda)=\lim_{\delta\lambda\to 0}|\langle\Psi_0(\lambda)|\Psi_i(\lambda+\delta\lambda)\rangle|^2/(\delta\lambda)^2$ (as the numerator converges to zero with $\delta\lambda\to 0$, the ratio yields a finite value). Summed over all levels, the total rate of mixing $\Sigma_i M_i(\lambda)\equiv M(\lambda)$ expresses the ''decay'' of the intermediate ground-state wave function under an infinitesimal variation of λ, namely, $|\langle\Psi_0(\lambda)|\Psi_0(\lambda+\delta\lambda)\rangle|^2\approx 1-M(\lambda)(\delta\lambda)^2$. It is given by

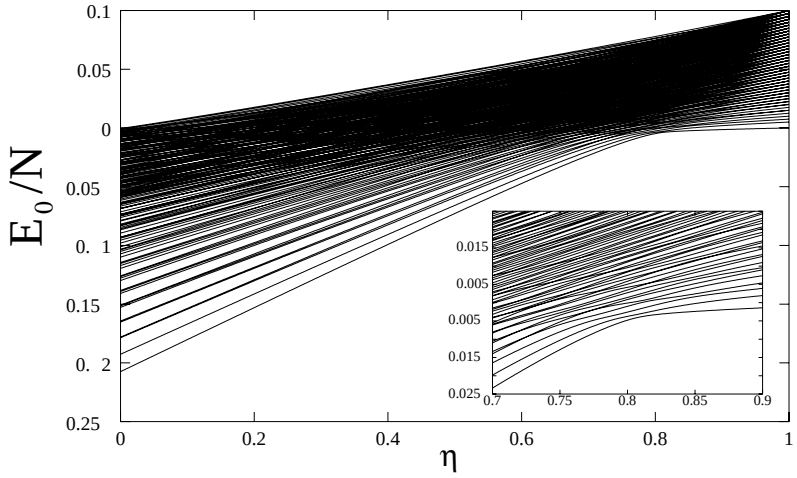

FIG. 9. Energies of all 0^+ states along paths A and $\overline{\mathrm{A}}$ for $N=40$. The inset shows a zoom into the low-energy phase-transitional region.

$$M(\lambda)=\sum_{i\neq 0}\frac{|\langle\Psi_i(\lambda)|V|\Psi_0(\lambda)\rangle|^2}{[E_i(\lambda)-E_0(\lambda)]^2}, \tag{20}$$

a very similar expression as Eq. (19), except for the power of energy denominators. These considerations shed more light on the link between the two definitions of the ''specific heat,'' as discussed above: the rate of change of the ground-state entropy with λ [measured by the derivative in Eq. (18), i.e., by the ''specific heat'' $c'(\lambda)$] is typically correlated with the decay rate of $|\Psi_0(\lambda)\rangle$, Eq. (20), and, therefore, it is expected to exhibit qualitatively similar behavior as $c(\lambda)$ in Eq. (19). This is what we indeed observe in panels (a) and (b) of Figs. 6 and 7. However, in spite of the link to Eq. (20) the quantity $c'(\lambda)$ cannot be exactly expressed in this or similar form. For instance, even rapid variations of the wave function due to a large mixing rate at a given λ do not have to necessarily induce substantial changes of the wave-function entropy in some reference bases. Therefore, the similarity of the corresponding curves in panels (a) and (b) of Figs. 6 and 7 is not perfect. In particular, the order of the phase transition, as determined from the variation of the ground-state energy, cannot be read out from the change of the ground-state wave-function entropy around the transitional point.

In Figs. 9, 10, and 11 we show the absolute energy of all 0^+ states for $N=40$ as a function of the varying parameter η or χ for transitional paths A/$\overline{\mathrm{A}}$, B, and C, respectively. These figures thus represent the dynamics of the whole ensemble of the Coulomb-gas particles along the respective transitions. One clearly sees that although the impulse of force at the phase-transitional point affects most the ground-state trajectory, the other levels are also involved, although in an extent decreasing with the excitation energy. This agrees with the understanding of the quantum phase transition as a simultaneous avoided crossing of a number of levels, indicated also by a peak in the distribution of the Hamiltonian's exceptional points [15,16,20]. The correlation between the level dynamics and mixing of wave functions implies that such places of multiple avoided crossings host sizeable structural changes of all the levels involved. The impact of such changes is far reaching and does not affect only the spectroscopy, as discussed in Sec. III B. For instance, consequences for quantum memory effects were investigated in Ref. [20].

Level dynamics along the three paths in Figs. 9–11 differ in one important aspect. While path B involves in its whole length integrable Hamiltonians [due to the underlying O(5) dynamical symmetry in both the O(6) and U(5) chains], paths A/$\overline{\mathrm{A}}$ and C are chaotic [59]. As a consequence, the

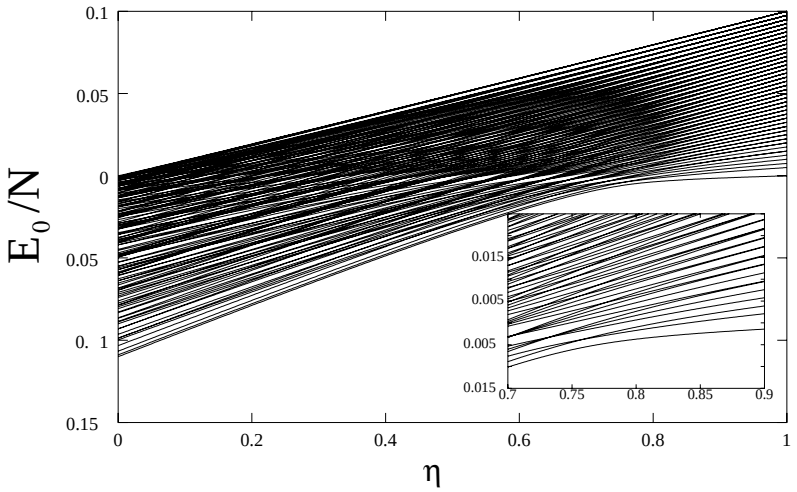

FIG. 10. The same as in Fig. 9, but for path B.

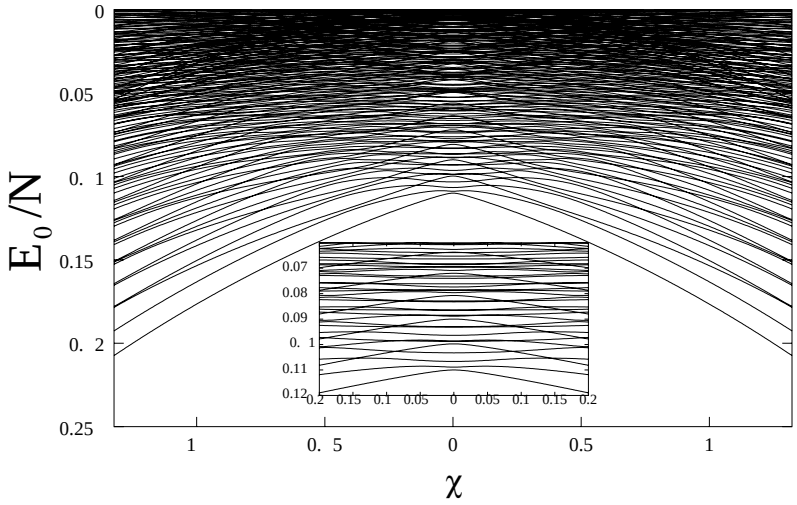

FIG. 11. The same as in Fig. 9, but for path C.

levels along path B (Fig. 10) cross each other for intermediate values of η with no induced repulsive forces (the corresponding charges vanish due to the underlying symmetry), while the levels along paths A/$\overline{\text{A}}$ and C can cross only in the dynamical-symmetry limits (away from the symmetries, the levels with the same angular momentum and parity do not typically cross since the varying control parameter η or χ is a single real variable). As an example, consider path C in Fig. 11. The level trajectories for this transition cross at the three dynamical symmetries involved, i.e., SU(3) (left), O(6) (middle), and $\overline{\text{SU(3)}}$ (right), which is due to the degeneracies connected with the SU(3), O(6), or $\overline{\text{SU(3)}}$ missing labels. However, as we can see in Fig. 11, avoided crossings away from integrable cases are still very close for large enough boson numbers.

Let us close this part by the remark that level dynamics along various transitional paths in the extended Casten triangle and its various consequences will be discussed in more detail in a forthcoming paper.

IV. EIGENSTATE MIXING AND THERMALIZATION

In the preceding section we attempted to attribute to the IBM ground state some appropriate ''thermal'' properties—specific heat, entropy, etc. Since these quantities are essentially applicable under statistical circumstances while the case studied represents a deterministic system, the above results just build up an *analogy* between the structural quantum phase transitions and standard thermodynamics. Let us stress that the actual specific heat of any quantum system at zero temperature (which corresponds to the situation studied here when only the ground state is populated) is identically zero in terms of thermodynamics. However, in this section we will discuss another framework for studying parameter-dependent quantum systems, such as the IBM, in which the thermal properties appear as a natural ingredient regardless of the actual population of the model eigenstates. The results obtained in this way will be closely related to those described above.

The statistical framework for studying a deterministic quantum system with external parameters utilizes the idea of randomization of the model Hamiltonian via a small stochastic component of the control parameters [21,60]. In this way, for instance, λ in Eq. (1) is subject to an external noise, $\lambda \rightarrow \lambda + \delta\lambda$, where $\delta\lambda$ is a zero-mean random variable with a small dispersion (relative to the range of λ). Usually we assume the Gaussian distribution $w(\delta\lambda) \propto \exp(-\delta\lambda^2/2\sigma^2)$ with $\sigma^2 = \langle \delta\lambda^2 \rangle \ll 1$. Accordingly, the Hamiltonian (1) acquires a random component

$$H(\lambda) \rightarrow H(\lambda + \delta\lambda) = H(\lambda) + \delta\lambda V, \tag{21}$$

where both deterministic and stochastic terms on the right-hand side are incompatible, $[H(\lambda), V] = [H_0, V] \neq 0$, the commutator showing no dependence on λ. The latter condition—as will be discussed below—is important and in fact restricts the use of this scheme only to linear Hamiltonians of form (1).

With the stochastic component, the ground state of the Hamiltonian (21) is not represented by a vector in the Hilbert space, but by a statistical ensemble of vectors, a density operator

$$|\Psi_0(\lambda)\rangle \rightarrow \varrho_0(\lambda) = \int w(\lambda')|\Psi_0(\lambda')\rangle\langle\Psi_0(\lambda')|d\lambda', \tag{22}$$

where we introduced $\lambda' = \lambda + \delta\lambda$ with $\langle \lambda' \rangle = \lambda$. The noise can be imagined as a random process, thus $\delta\lambda$ dependent on time, whose dynamics is very slow (adiabatic) with respect to the periodic motion associated with the ground state. Then the statistical ensemble in Eq. (22) represents states of the randomly driven system (in the lowest-energy state) that actually occur in time with the respective weights.

The density operator (22) involves the ''statistical element'' needed for a fundamentally motivated assignment of thermal properties to a given deterministic system. Namely [21], it can be associated with a canonical density operator $\varrho_{\text{th}}(\lambda) = \exp[-\mathcal{H}(\lambda)/T(\lambda)]/Z(\lambda)$, where Z is the partition sum while $\mathcal{H}$ and T stand for a ''fictitious'' Hamiltonian and an effective temperature, respectively, both attributed to the density operator (22) via the required equality $\varrho_0(\lambda) = \varrho_{\text{th}}(\lambda)$. As shown in Ref. [21], an inherent ambiguity of

the thermal density operator associated with the original density matrix in Eq. (22) makes it possible to fix the energy average $\langle E\rangle$ and dispersion $\langle E^2\rangle-\langle E\rangle^2$ of $\varrho_{\rm th}$ to the respective values corresponding to ϱ_0. Consequently, one obtains the relation $\langle E^2\rangle-\langle E\rangle^2=c_{\rm th}T^2$, where $c_{\rm th}$ is the specific heat of the thermally populated system (i.e., the system represented by the Hamiltonian $\mathcal{H}$), which is—at the same time—expressed through ϱ_0:

$$c_{\rm th}(\lambda)={\rm Tr}[\varrho_0(\lambda)\ln^2\varrho_0(\lambda)]-{\rm Tr}^2[\varrho_0(\lambda)\ln\varrho_0(\lambda)]. \tag{23}$$

We thus obtain yet another definition of the ''specific heat'' than those discussed in Sec. III.

The density operator $\varrho_0(\lambda)$ and thus also the ''specific heat'' (23) depend on fluctuations of the model control parameter, i.e., on $w(\delta\lambda)$. As this distribution is assumed to have the Gaussian form, we have one free parameter σ^2 involved in the analysis. The requirement of $\sigma^2\ll 1$ makes the perturbative treatment applicable [21,60], which results in the leading-order term of the ''specific heat'' from Eq. (23) given by the following expression:

$$c_{\rm th}(\lambda)\approx(\sigma^2\ \ln^2\ \sigma^2)M(\lambda)+\cdots. \tag{24}$$

Here, $M(\lambda)$ is the rate of mixing from Eq. (20) and the dots stand for terms which can be neglected in comparison with the present term for $\sigma^2\to 0$. We see that in this limit the ''specific heat'' has a nonanalytical behavior, so that anyhow small noise $\sigma^2>0$ produces a finite value of $c_{\rm th}$. Moreover, the ''specific heat'' for small fluctuations is approximately proportional to the total rate of mixing of the given state with the other states, in a close correspondence with results discussed in Sec. III. In particular, Eq. (24) ensures a peaked behavior of the ''specific heat'' (23) at phase transitions, as we explicitly demonstrate below. This all gives the present randomization scheme with small-amplitude noise deeper physical sense.

As mentioned above, the randomization in Eq. (21) requires a linear dependence of the original Hamiltonian on the control parameter subject to the noise. In the opposite case, the rate of mixing generated by the noise may undergo ''secular'' variations with λ, since a degree of incompatibility of the deterministic and statistical terms in the Hamiltonian changes with λ. For instance, the randomization of the χ dependence of the Hamiltonian (8) would imply that $H(\chi+\delta\chi)$ (for now we skip η from the notation) is given by a more complicated form than Eq. (21), namely by $H(\chi)+\delta\chi H'(\chi)+\delta\chi^2H''$, where the commutator of the statistical terms $\delta\chi H'(\chi)$ and $\delta\chi^2H''$ (their explicit form can be easily calculated) with the deterministic term $H(\chi)$ varies with χ. On the other hand, the randomization of the η dependence in Eq. (8) works as explained above, the statistical term $\delta\eta V$ given by Eq. (14). We therefore present here calculations of the ''specific heat'' according to the randomization scheme only for paths A/$\overline{\rm A}$ and B. These are given in Figs. 6(c) and 7(c) for $N=10,\ldots,40$, where the dispersion of the Gaussian random variable $\delta\eta$ was varied with the boson number as $\sigma^2=10^{-4}\times(10/N)^{1.2}$.

The dependence of the noise amplitude σ on N, as employed in calculations shown in panel (c) of Figs. 6 and 7, results from an optimal fit of the present specific heat $c_{\rm th}(\lambda)$ to $c(\lambda)$ from Eq. (17) for path B. Indeed, the shapes of all curves for $N=10,\ldots,40$ in panel (c) of Fig. 7 are very similar, in fact practically indistinguishable, from the respective curves in panel (a). However, because the formulas leading the behavior in both cases are similar but not identical, see Eqs. (24) and (19), the unification of the two sets of curves cannot be quite universal, as exemplified by shape differences for paths A/$\overline{\rm A}$ shown in panels (a) and (c) of Fig. 6, where we used the same scaling of σ^2 with N as for path B.

Another approach to determine a suitable ansatz for the dependence of σ^2 on N can be derived from the theory of parametric decorrelations of wave functions [61], which yields predictions for an average overlap $|\langle\Psi_i(\lambda)|\Psi_i(\lambda+\delta\lambda)\rangle|^2$ in terms of a universally scaled control parameter. It turns out [61] that the overlap depends in a generic way on $\widetilde{\delta\lambda}=\sqrt{D}\,\delta\lambda$, where D is a ''diffusion constant'' for level energies. As in our case these energies are globally proportional to N, thus $D\propto N^2$, one could argue for the $\sigma^2\propto 1/N^2$ scaling of the size of fluctuations. In this case, results of the above calculations with different boson numbers should be comparable. Indeed, we checked that for this scaling the N-dependent curves of the ''specific heat'' according to Eq. (23) peak with approximately the same maximum value at the phase transition and sharpen as N increases. However, to show the similarity of forms for different definitions of the ''specific heat'' we present in Figs. 6(c) and 7(c) the curves with the empirical scaling, as discussed above.

It is interesting to realize that the present randomization scheme offers several alternative possibilities for definitions of the ''specific heat.'' Having introduced the density operator in Eq. (22), one can, for example, determine von Neumann entropy $S_0=-{\rm Tr}[\varrho_0\ln\varrho_0]$ and calculate the ''specific heat'' from its first derivative with respect to the control parameter. This quantity, however, would not have the characteristic form with a peak locating the phase transition, since von Neumann entropy itself is already peaked at the phase transition. Details, including a discussion of differences between $c_{\rm th}$ and S_0, can be found in Ref. [21].

Nevertheless, the randomization scheme in the IBM case yields another entropic quantity which has a steplike behavior at the phase transition and thus results in a peaked form of the ''specific heat.'' This quantity is the overlap entropy of the density-operator eigenbasis with eigenbases of conveniently chosen Hamiltonians [21]. The eigenbasis $\{|\Phi_i(\lambda)\rangle\}$ of the density operator in Eq. (22) at a given λ is obtained simply by the diagonalization of $\varrho_0(\lambda)$ and has in general nothing to do with the Hamiltonian eigenbases $\{|\Psi_i(\lambda')\rangle\}$ at any λ', except being, of course, another orthonormal basis of the whole n-dimensional Hilbert space of states. The overlap entropy measures the proximity of the ϱ_0 eigenbasis—in another context also called the ''pointer basis''—to an arbitrary basis $\mathcal{B}\equiv\{|i^{\mathcal{B}}\rangle\}$ through the following formula:

$$O_0^{\mathcal{B}}(\lambda)=-\frac{1}{n}\sum_j\ \sum_i\ |\langle\Phi_j(\lambda)|i^{\mathcal{B}}\rangle|^2\ln|\langle\Phi_j(\lambda)|i^{\mathcal{B}}\rangle|^2. \tag{25}$$

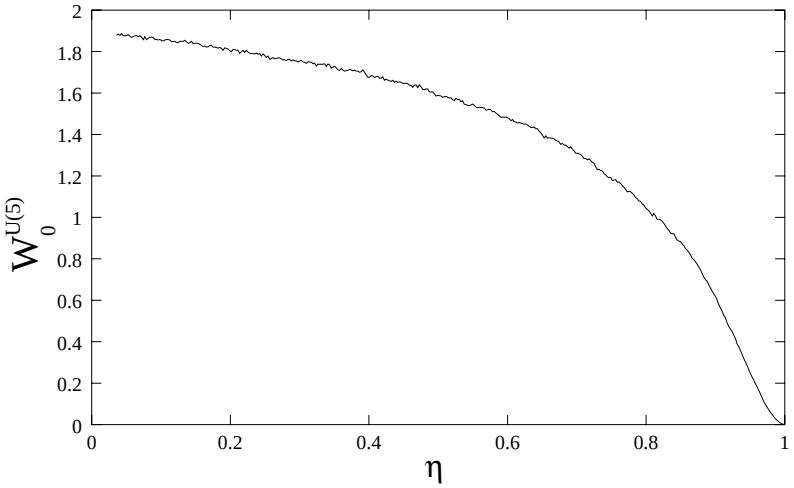

FIG. 12. The U(5) overlap entropy of the ϱ_0 eigenbasis as a function of η for path B and $N=40$.

We see that this is just the average wave-function entropy of all the density-matrix eigenstates in the reference basis $\mathcal{B}$, cf. Eq. (16).

A natural choice for $\mathcal{B}$ in Eq. (25) is either (a) the local eigenbasis of $H(\lambda)$, i.e., the energy eigenbasis $\mathcal{B}_{H(\lambda)}=\{|\Psi_i(\lambda)\rangle\}$ at the same value of control parameters as where the basis of $\varrho_0(\lambda)$ is taken from (in the IBM case λ stands for both η and χ), or (b) the Hamiltonian eigenbases corresponding to the dynamical symmetries of the model. Of the latter possibilities, only the U(5) dynamical-symmetry basis $\mathcal{B}_{\mathrm{U}(5)}$ turns out interesting. In both of these cases, $\mathcal{B}=\mathcal{B}_{H(\lambda)}$ and $\mathcal{B}_{\mathrm{U}(5)}$, the overlap entropy with the pointer basis was shown [21] to decrease to zero close to the U(5) vertex of the Casten triangle, the spherical-deformed phase separatrix again defining approximately the zone of maximal change of the corresponding entropies. We must emphasize that the other dynamical-symmetry bases turn out totally irrelevant for the ϱ_0 eigenbasis since their overlap entropies—regardless of whether they are evaluated in a close vicinity to the respective symmetry or anywhere else—were checked to have similar values as expected just for any randomly chosen basis [21].

Therefore, in analogy with Eq. (18), we can introduce another ''specific heat''

$$c'_{\mathrm{th}}(\eta)|_\chi = -\frac{\partial}{\partial\eta}O_0^{\mathcal{B}}(\eta,\chi), \tag{26}$$

where $\mathcal{B}=\mathcal{B}_{\mathrm{U}(5)}$. It is shown in panel (d) of Figs. 6 (for paths A/$\overline{\mathrm{A}}$) and 7 (path B), again with $N=10,\ldots,40$ (the scaling of σ^2 with N remains the same as above). In the phase-transitional region, $\eta\in(0.7,1)$, all curves with $N>10$ exhibit a clear maximum whose height increases with the boson number. Thus the corresponding overlap entropy is a sharply decreasing function of η in this interval, see an example in Fig. 12 (the sharpness increases as approaching the asymptotic regime). Let us note that the irregularities observed particularly on lower-N curves shown in Figs. 6(d) and 7(d) result from some numerical instabilities connected with the precise diagonalization of the density matrix ϱ_0 for very small noise.

An interesting observation, resulting from detailed calculations that we do not show here, is that when approaching the U(5) limit along both paths A/$\overline{\mathrm{A}}$ and B (and also the other paths in between), the ϱ_0 eigenbasis at intermediate values of the control parameter is even closer to the U(5) basis than to the local energy eigenbasis $\mathcal{B}_{H(\lambda)}$. This is indicated by a faster decrease of the U(5) overlap entropy in comparison to the overlap entropy with $\mathcal{B}_{H(\lambda)}$. Thus the ''attraction'' of the density-matrix eigenbasis to the U(5) basis close to this limit seems to be the major effect, while the decrease of the $\mathcal{B}_{H(\lambda)}$ overlap entropy comes only as a consequence due to the convergence of $\mathcal{B}_{H(\lambda)}$ to $\mathcal{B}_{\mathrm{U}(5)}$. Recall that, fundamentally, there is no need for such an attraction and—as pointed out for one special case already in Ref. [21]—the behavior observed in Figs. 6(d) and 7(d) is indeed an exceptional property of transitions to the U(5) symmetry. So far, no explanation was found for this phenomenon, although it seems to be an analog of the similar behavior of the U(5) wave-function entropy in the IBM without randomization (Sec. III).

V. CONCLUSIONS

Let us summarize the main conclusions of this work: First, we reviewed and compared—in Sec. II—various ways of how geometry and shape-phase transitions can be studied in low-energy nuclear physics. Except the phenomenological geometric model (Sec. II A), the central role in all approaches is played by the algebraic method and condensate/coherent trial states (Secs. II B and II C). We saw that Eq. (3) represents a universal result so that the analysis in the framework of Landau theory, e.g., Fig. 1(a), is relevant regardless of the concrete model used. In particular, phase transitions between axially symmetric deformed and spherical, and between prolate and oblate shapes of the ground state appear in all algebraic models with quadrupole variables, the axial symmetry resulting from the form of the model Hamiltonian with at most two-body terms. Triaxiality and the corresponding phase transitions can nevertheless occur, as shown in Ref. [14] using the FDSM, if the available range in the $\beta\times\gamma$ plane is restricted by a microscopic analysis.

Second, we demonstrated on several examples that suitably selected quantum signatures of shape-phase transitions make it possible to detect the transition and locate a given nucleus in its vicinity even in situations when the sharp phase-transitional behavior is smoothened by fluctuations in finite systems (see Sec. III B). The calculation of selected observables was performed across the whole extended Casten triangle of the IBM control parameters for boson numbers going up to previously unreachable values, even $N=80$, see Figs. 4 and 5.

Third, we introduced and analyzed several quantities that can for nuclear ground-state shape-phase transitions be considered analogous to the specific heat in standard thermodynamics—see Sec. III C. In particular, the second derivative of the ground-state energy, $c(\lambda)$ in Eq. (17), and the first derivative of the U(5) (for paths A/$\overline{\text{A}}$ and B) or SU(3) (for path C) wave-function entropy, $c'(\lambda)$ in Eq. (18), were shown to play that role in the IBM. These quantities proved to be extremely sensitive to the phase-transitional effects and their washing out at finite boson numbers. Equations (19) and (20) provide the insight needed for fundamental understanding of the similarity exhibited by peaked forms of the ''specific heats,'' see panels (a) and (b) of Figs. 6–8. The ''coming together'' of all the levels at the phase-transitional point, see Figs. 9–11, or ''multiple avoided crossing'' in a more sophisticated language, is associated with the crossover effects on wave functions, as already discussed before for numerous quantum systems [15–21].

Finally, in Sec. IV we discussed and utilized the general randomization scheme for Hamiltonians with a linear dependence on control parameters. Through this scheme, statistical and thermal properties of otherwise deterministic quantum systems can be naturally introduced. Two additional definitions of the ''specific heat'' were considered, namely, the one derived from the energy dispersion of the randomized system, $c_{\text{th}}(\lambda)$ in Eq. (23), and the other based on the overlap entropy of the pointer basis with the U(5) basis, $c'_{\text{th}}(\lambda)$ in Eq. (26). We saw that mixing properties of energy eigenstates are again of the major importance for outputs of the randomization method—see, e.g., Eq. (24) which leads to very similar behavior of $c_{\text{th}}(\eta)$ in panel (c) of Figs. 6 and 7 with $c(\eta)$ and $c'(\eta)$ in panels (a) and (b). An important issue in this respect is the scaling of the range of fluctuations $\delta\lambda$ with N.

The quantities $c'(\lambda)$, $c_{\text{th}}(\lambda)$, and $c'_{\text{th}}(\lambda)$ discussed above represent a nontrivial generalization of the ''specific heat'' $c(\lambda)$ from Eq. (17). While $c(\lambda)$ was introduced as a direct analog of the specific heat in standard thermodynamics, the other definitions are either based on the first derivative of an entropic quantity [$c'(\lambda)$ and $c'_{\text{th}}(\lambda)$], or represent actual specific heat of a ''thermal equivalent'' associated with the given randomized system [$c_{\text{th}}(\lambda)$]. Their comparison on the same basis is thus fully justified. The verification of their peaked form at the structural phase transitions, Figs. 6–8, is therefore the main result of the present work, indicating far-reaching analogies between thermodynamics and nonstatistical quantum mechanics. It consistently extends the recent application [34] of the Landau theory of phase transitions in the analysis of behaviors encoded in the energy functional (6). Let us note that while the ''specific heat'' $c_{\text{th}}(\lambda)$ in Eq. (23) is rather universal, as discussed already in Ref. [21], the definition of $c'_{\text{th}}(\lambda)$ in Eq. (26) concerns the IBM only. In particular, the reason for the decrease of the U(5) overlap entropy with η, see Fig. 12, and thus also for the peaked form of the $c'_{\text{th}}(\eta)$ curves remains basically unclear; we verified here that the effect first observed in Ref. [21] concerns also the other transitional paths to the U(5) symmetry.

Let us stress that in this paper we focused on properties of the ground state only. The structure of the ground state is clearly substantial for the main features of all low-energy collective states. However, the techniques discussed here could equally well be employed also at higher excitations, either by explicitly focusing on particular excited states, or via introducing a canonical population of the model states with finite temperatures. Note that some of these results were already discussed in previous papers [20,21] and showed that the phase-transitional behavior persists in a limited part of the IBM spectrum above the ground state.

We believe that structural phase transitions in finite quantum systems, such as atomic nuclei, represent important and interesting subject of contemporary many-body physics.

ACKNOWLEDGMENTS

The authors thank R. Bijker, R.F. Casten, F. Iachello, A. Linnemann, A. Schiller, P. Stránský, P. von Brentano, V. Werner, and V. Zelevinsky for illuminating discussions. The work was supported by the DFG under Grant No. 436 TSE 17/04/02 and by the GAČR under Grant No. 202/02/0939. P.C. acknowledges the University of Cologne for the hospitality and excellent working environment.

[1] H. E. Stanley, *Introduction to Phase Transitions and Critical Phenomena* (Oxford University Press, Oxford, England, 1971).
[2] S. Sachdev, *Quantum Phase Transitions* (Cambridge University Press, Cambridge, England, 1999).
[3] H. Meyer-Ortmanns, Rev. Mod. Phys. **68**, 473 (1996).
[4] J. Pochodzalla *et al.*, Phys. Rev. Lett. **75**, 1040 (1995); M. D'Agostino *et al.*, Phys. Lett. B **473**, 219 (2000).
[5] J.J. Gaardhøje, C. Ellegaard, B. Herskind, and S.G. Steadman, Phys. Rev. Lett. **53**, 148 (1984); C.A. Gossett, K.A. Snover, J.A. Behr, G. Feldman, and J.L. Osborne, *ibid.* **54**, 1486 (1985); R. Holzmann *et al.*, *ibid.* **62**, 520 (1989).
[6] M. Brack and P. Quentin, Phys. Lett. **52B**, 159 (1974).
[7] S. Levit and Y. Alhassid, Nucl. Phys. **A413**, 439 (1984); Y. Alhassid, S. Levit, and J. Zingman, Phys. Rev. Lett. **57**, 539 (1986); Y. Alhassid, J. Zingman, and S. Levit, Nucl. Phys. **A469**, 205 (1987); Y. Alhassid and B. Bush, *ibid.* **A549**, 12 (1992).
[8] B. Mottelson and J. Valantin, Phys. Rev. Lett. **5**, 511 (1960); A.L. Goodman, Nucl. Phys. **A369**, 365 (1981); M. Guttormsen, M. Hjorth-Jensen, E. Melby, J. Rekstad, A. Schiller, and S.

Siem, Phys. Rev. C **64**, 034319 (2001); S. Liu and Y. Alhassid, Phys. Rev. Lett. **87**, 022501 (2001).
[9] D.J. Thouless, Nucl. Phys. **22**, 78 (1961).
[10] A.E.L. Dieperink, O. Scholten, and F. Iachello, Phys. Rev. Lett. **44**, 1747 (1980); A.E.L. Dieperink and O. Scholten, Nucl. Phys. **A346**, 125 (1980).
[11] D.H. Feng, R. Gilmore, and S.R. Deans, Phys. Rev. C **23**, 1254 (1981).
[12] E.D. Davis and W.D. Heiss, J. Phys. G **12**, 805 (1986).
[13] W.-M. Zhang, D.H. Feng, and J.N. Ginocchio, Phys. Rev. Lett. **59**, 2032 (1987); Phys. Rev. C **37**, 1281 (1988).
[14] W.-M. Zhang, C.-L. Wu, D.H. Feng, J.N. Ginocchio, and M.W. Guidry, Phys. Rev. C **38**, 1475 (1988).
[15] W.D. Heiss, Z. Phys. A **329**, 133 (1988); W.D. Heiss and A.A. Kotzé, *ibid.* **331**, 223 (1988).
[16] W.D. Heiss and A.L. Sannino, Phys. Rev. A **43**, 4159 (1991); W.D. Heiss, Phys. Rep. **242**, 443 (1994); W.D. Heiss and M. Müller, Phys. Rev. E **66**, 016217 (2002).
[17] I.Kh. Zharekeshev and B. Kramer, Phys. Rev. B **51**, 17 239 (1995).
[18] W.D. Heiss, M. Müller, and I. Rotter, Phys. Rev. E **58**, 2894 (1998); C. Jung, M. Müller, and I. Rotter, *ibid.* **60**, 114 (1999).
[19] D.J. Rowe, C. Bahri, and W. Wijesundera, Phys. Rev. Lett. **80**, 4394 (1998).
[20] P. Cejnar and J. Jolie, Phys. Rev. E **61**, 6237 (2000).
[21] P. Cejnar, V. Zelevinsky, and V.V. Sokolov, Phys. Rev. E **63**, 036127 (2001).
[22] C. Emary and T. Brandes, Phys. Rev. Lett. **90**, 044101 (2003).
[23] R.F. Casten, N.V. Zamfir, and D.S. Brenner, Phys. Rev. Lett. **71**, 227 (1993).
[24] E. López-Moreno and O. Castaños, Phys. Rev. C **54**, 2374 (1996).
[25] F. Iachello, N.V. Zamfir, and R.F. Casten, Phys. Rev. Lett. **81**, 1191 (1998).
[26] J. Jolie, P. Cejnar, and J. Dobeš, Phys. Rev. C **60**, 061303(R) (1999).
[27] R.F. Casten, D. Kusnezov, and N.V. Zamfir, Phys. Rev. Lett. **82**, 5000 (1999).
[28] F. Iachello, Phys. Rev. Lett. **85**, 3580 (2000); **87**, 052502 (2001).
[29] R.F. Casten and N.V. Zamfir, Phys. Rev. Lett. **85**, 3584 (2000); **87**, 052503 (2001).
[30] J.E. García-Ramos, D. De Coster, R. Fossion, and K. Heyde, Nucl. Phys. **A688**, 735 (2001).
[31] J. Jolie, R.F. Casten, P. von Brentano, and V. Werner, Phys. Rev. Lett. **87**, 162501 (2001); J. Jolie and A. Linnemann, Phys. Rev. C **68**, 031301 (2003).
[32] J. Jolie, S. Heinze, P. von Brentano, V. Werner, and P. Cejnar, in *Mapping the Triangle*, edited by Ani Aprahamian, Jolie A. Cizewski, Stuart Pittel, and N. Victor Zamfir, AIP Conf. Proc. **638** (AIP, Melville, NY, 2002), p. 213.
[33] V. Werner, P. von Brentano, R.F. Casten, and J. Jolie, Phys. Lett. B **527**, 55 (2002).
[34] J. Jolie, P. Cejnar, R.F. Casten, S. Heinze, A. Linnemann, and V. Werner, Phys. Rev. Lett. **89**, 182502 (2002).
[35] P. Cejnar, Phys. Rev. C **65**, 044312 (2002); Phys. Rev. Lett. **90**, 112501 (2003).
[36] F. Iachello and A. Arima, *The Interacting Boson Model* (Cambridge University Press, Cambridge, England, 1987).
[37] J. M. Eisenberg and W. Greiner, *Nuclear Models* Nuclear Theory Vol. 1, (North-Holland, Amsterdam, 1987).
[38] A. Bohr and B. Mottelson, *Nuclear Structure* (Benjamin, Reading, Mass, 1975), Vol. II.
[39] L. Landau, Phys. Z. Sowjetunion **11**, 26 (1937); **11**, 545 (1937); reprinted in *Collected Papers of L. D. Landau* (Pergamon, Oxford, 1965), p. 193.
[40] L. D. Landau and E. M. Lifshitz, *Statistical Physics*, Course of Theoretical Physics Vol. V (Butterworth, Oxford, 2001).
[41] R. Gilmore, Ann. Phys. (N.Y.) **74**, 391 (1972); A.M. Perelomov, Commun. Math. Phys. **26**, 222 (1972).
[42] J.N. Ginocchio and M.W. Kirson, Phys. Rev. Lett. **44**, 1744 (1980); Nucl. Phys. **A350**, 31 (1980).
[43] P. Van Isacker and J.-Q. Chen, Phys. Rev. C **24**, 684 (1981).
[44] R.L. Hatch and S. Levit, Phys. Rev. C **25**, 614 (1982).
[45] P. Van Isacker, A. Frank, and J. Dukelsky, Phys. Rev. C **31**, 671 (1985).
[46] A.M. Shirokov, N.A. Smirnova, and Yu.F. Smirnov, Phys. Lett. B **434**, 237 (1998).
[47] P. Cejnar and H.B. Geyer, Phys. Rev. C **64**, 034307 (2001).
[48] J. Dobeš, Phys. Rev. C **42**, 2023 (1990).
[49] A. Klein and E.R. Marshalek, Rev. Mod. Phys. **63**, 375 (1991).
[50] J.N. Ginocchio, Ann. Phys. (N.Y.) **126**, 234 (1980).
[51] C.-L. Wu, D.H. Feng, X.-G. Chen, J.-Q. Chen, and M.W. Guidry, Phys. Lett. **168B**, 313 (1986); Phys. Rev. C **36**, 1157 (1987).
[52] G.K. Kim and C.M. Vincent, Phys. Rev. C **35**, 1517 (1987).
[53] H. B. Geyer, F. J. W. Hahne, and F. G. Scholtz, in *Understanding the Variety of Nuclear Excitations*, edited by A. Covello (World Scientific, Singapore, 1991), p. 291.
[54] H.B. Geyer, F.J.W. Hahne, and F.G. Scholtz, Phys. Rev. Lett. **58**, 459 (1987).
[55] F.M. Izrailev, Phys. Lett. A **134**, 13 (1988); J. Jolie, in *Perspectives for the Interacting Boson Model*, edited by R. F. Casten *et al.* (World Scientific, Singapore, 1994), p. 45; V. Zelevinsky, M. Horoi, and B.A. Brown, Phys. Lett. B **350**, 141 (1995); M. Horoi, V. Zelevinsky, and B.A. Brown, Phys. Rev. Lett. **74**, 5194 (1995).
[56] P. Cejnar and J. Jolie, Phys. Lett. B **420**, 241 (1998); Phys. Rev. E **58**, 387 (1998).
[57] P. Pechukas, Phys. Rev. Lett. **51**, 943 (1983); T. Yukawa, *ibid.* **54**, 1883 (1985).
[58] P. Gaspard, S.A. Rice, H.J. Mikeska, and K. Nakamura, Phys. Rev. A **42**, 4015 (1990); J. Zakrzewski and D. Delande, Phys. Rev. E **47**, 1650 (1993).
[59] N. Whelan and Y. Alhassid, Nucl. Phys. **A556**, 42 (1993).
[60] V.V. Sokolov, B.A. Brown, and V. Zelevinsky, Phys. Rev. E **58**, 56 (1998).
[61] D. Mitchell, Y. Alhassid, and D. Kusnezov, Phys. Lett. B **215**, 21 (1996); D. Kusnezov and D. Mitchell, Phys. Rev. C **54**, 147 (1996); D. Kusnezov, B.A. Brown, and V. Zelevinsky, Phys. Lett. B **365**, 5 (1996).